UCSF
UC San Francisco Previously Published Works

Title

Synthesis and single-molecule imaging reveal stereospecific enhancement of binding kinetics by the antitumour eEF1A antagonist SR-A3

Permalink

https://escholarship.org/uc/item/6897m8d7

Journal

Nature Chemistry, 14(12)

ISSN

1755-4330

Authors

Wang, Hao-Yuan
Yang, Haojun
Holm, Mikael
et al.

Publication Date

2022-12-01

DOI

10.1038/s41557-022-01039-3

Peer reviewed

eScholarship.org Powered by the California Digital Library
University of California

Author Manuscript

Author Manuscript

Author Manuscript

Author Manuscript

HHS Public Access

Author manuscript

Nat Chem. Author manuscript; available in PMC 2023 June 01.

Published in final edited form as:

Nat Chem. 2022 December ; 14(12): 1443–1450. doi:10.1038/s41557-022-01039-3.

Synthesis and single-molecule imaging reveal stereospecific enhancement of binding kinetics by the antitumour eEF1A antagonist SR-A3

Hao-Yuan Wang[†], **Haojun Yang**[‡,#], **Mikael Holm**[¤,#], **Harrison Tom**[‡], **Keely Oltion**[†], **Amjad Ayad Qatran Al-Khdhairawi**[§], **Jean-Frédéric F. Weber**[¶], **Scott C. Blanchard**[¤], **Davide Ruggero**[†,‡], **Jack Taunton**[†,*]

[†]Department of Cellular and Molecular Pharmacology, University of California, San Francisco, CA 94158, United States

[‡]Department of Urology, University of California, San Francisco, CA 94158, United States

[¤]Department of Structural Biology, St. Jude Children's Research Hospital, Memphis, TN 38105, United States

[§]School of Pharmacy, Faculty of Health & Medical Sciences, Taylor's University Lakeside Campus, 47500 Subang Jaya, Selangor, Malaysia

[¶]Atta-ur-Rahman Institute for Natural Product Discovery (AuRIns), Universiti Teknologi MARA (UiTM) Selangor Branch, 42300 Bandar Puncak Alam, Selangor, Malaysia

Abstract

Ternatin-family cyclic peptides inhibit protein synthesis by targeting the eukaryotic elongation factor-1α (eEF1A). A potentially related cytotoxic natural product ("A3") was isolated from Aspergillus, but only 4 of its 11 stereocenters could be assigned. Here, we synthesized SR-A3 and SS-A3 – two out of 128 possible A3 epimers – and discovered that synthetic SR-A3 is indistinguishable from naturally derived A3. Relative to SS-A3, SR-A3 exhibits enhanced residence time and rebinding kinetics, as revealed by single-molecule fluorescence imaging of elongation reactions catalyzed by eEF1A in vitro. Increased residence time – stereospecifically conferred by the unique β-hydroxyl in SR-A3 – was also observed in cells. Consistent with its prolonged duration of action, thrice-weekly dosing with SR-A3 led to reduced tumor burden and increased survival in an aggressive Myc-driven mouse lymphoma model. Our results demonstrate

[*]Corresponding author: jack.taunton@ucsf.edu.

[#]These authors contributed equally: Haojun Yang, Mikael Holm

Author Contributions

H.Y.W. and J.T. conceived the project, designed the experiments, and analyzed the data. H.Y.W. synthesized, characterized, and tested the compounds in cellular experiments. H.Y.W. and K.O. performed OPP incorporation experiments. H.Y. and H.T. performed mouse experiments. M.H. acquired and analyzed smFRET data. A.A.Q.A.K. and J.F.W. isolated natural A3. D.R. and S.C.B. helped analyze data from the mouse lymphoma and smFRET experiments, respectively. H.Y.W. and J.T. wrote the manuscript with input from all of the authors.

Competing Interests

H.Y.W., H.Y., K.O., D.R., and J.T. are listed as inventors on a patent application covering SR-A3 (PCT/US2021/016790, patent pending). S.C.B. holds equity interests in Lumidyne Technologies. D.R. is a shareholder of eFFECTOR Therapeutics, Inc. and is a member of its scientific advisory board. J.T. is a founder of Global Blood Therapeutics, Kezar Life Sciences, Cedilla Therapeutics and Terremoto Biosciences, and is a scientific advisor to Entos.

Author Manuscript Author Manuscript Author Manuscript Author Manuscript

the potential of SR-A3 as a cancer therapeutic and exemplify an evolutionary mechanism for enhancing cyclic peptide binding kinetics via stereospecific side-chain hydroxylation.

Graphical Abstract

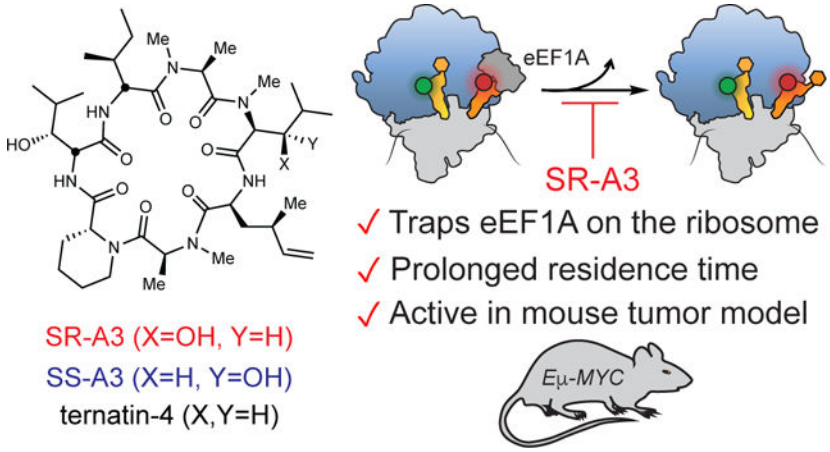

Introduction

All living organisms rely on protein synthesis mediated by the ribosome and its associated translation factors. Bacterial ribosomes have long been targeted by small-molecule antimicrobials,[1] while the human ribosome and translation factors have recently emerged as promising drug targets for cancer and viral infections.[2,3] Eukaryotic elongation factor-1α (eEF1A) is an essential component of the translation machinery.[4] GTP-bound eEF1A delivers aminoacyl-transfer RNAs (aa-tRNA) to the ribosomal A site during the elongation phase of protein synthesis. Base pairing between the A-site mRNA codon and the aa-tRNA anticodon promotes GTP hydrolysis by eEF1A, releasing the aa-tRNA from eEF1A and allowing its accommodation into the ribosome. The growing protein chain is subsequently transferred from the P-site peptidyl tRNA to the A-site aa-tRNA, extending it by one amino acid through ribosome-catalyzed peptide bond formation.

Tumor cells and viruses highjack the protein synthesis machinery to elicit growth and replication. Specific eEF1A inhibitors – all of which are macrocyclic natural products – have been evaluated as potential anticancer and antiviral drugs.[5] Didemnin B,[6,7] cytotrienin A,[8] nannocystin A,[9] and cordyheptapeptide A[10] are examples of structurally diverse macrocycles that bind eEF1A and inhibit translation elongation. Dehydro-didemnin B (plitidepsin) is approved in Australia for the treatment of relapsed/refractory multiple myeloma[11] and is efficacious in SARS-CoV-2 infection models.[12]

The cyclic heptapeptide A3 was isolated from an Aspergillus strain on the basis of its ability to inhibit cancer cell proliferation at low nanomolar concentrations.[13] Although the amino acid composition, sequence, and *N*-methylation pattern of A3 were deduced, only 4 out of 11 stereocenters could be assigned (Figure 1). Motivated by its potent antiproliferative activity and unknown mechanism of action, we sought to determine which of the 128 possible stereoisomers (based on 7 unassigned stereocenters) corresponds to A3. Based

Author Manuscript Author Manuscript Author Manuscript Author Manuscript

on our observation that the amino acid sequence and *N*-methylation pattern of A3 and ternatin are similar,[14] we previously designed and synthesized ternatin-4, which incorporates the dehydromethyl leucine (dhML) and pipecolic acid residues found in A3, yet lacks the β-hydroxy group attached to *N*-Me-Leu (Figure 1). We discovered that ternatin-4 inhibits cancer cell proliferation and SARS-CoV-2 replication by targeting eEF1A.[15,16] However, the precise step(s) of eEF1A-catalyzed elongation blocked by ternatin-family cyclic peptides – as well as the structure of A3 and the role of its unique β-hydroxy group – all remain unknown.

Here, we report the first total syntheses of two A3 epimers, SR-A3 and SS-A3 (Figure 1), along with cellular and single-molecule biophysical studies focused on quantifying drug-target residence times. Synthetic SR-A3 potently inhibited cell proliferation and protein synthesis by targeting eEF1A and was spectroscopically and biologically indistinguishable from the natural product A3. Transient exposure of cells to SR-A3 resulted in long-lasting inhibitory effects, whereas similarly prolonged effects were not observed with SS-A3 or ternatin-4. To gain mechanistic insight into these differences, we assessed eEF1A-catalyzed translation via single-molecule fluorescence resonance energy transfer (smFRET) imaging. These experiments directly revealed SR-A3's comparatively long duration of eEF1A blockade on the ribosome, enabled in part by its enhanced capacity to rebind following dissociation. Preclinical studies in a mouse model of human Burkitt lymphoma revealed that SR-A3, but not ternatin-4, exhibits potent antitumour activity. Our data thus reveal a striking and stereospecific enhancement in eEF1A binding kinetics conferred by a single oxygen atom appended to a cyclic peptide.

Results

Synthesis of SR-A3 and SS-A3 via an expeditious route to dehydromethyl-Leu

We speculated that dehydromethyl leucine (hereafter "dhML") in the natural product A3 has the same stereochemistry as in the synthetic compound, ternatin-4 (Figure 1). Because our original 6-step synthesis of dhML methyl ester was low yielding and required a costly chiral auxiliary, we developed a more efficient, second-generation synthesis suitable for preparing gram quantities of Fmoc-dhML.

Copper(I)-promoted S_N2' reaction of a serine-derived organozinc reagent with allylic electrophiles has been previously used to synthesize amino acids that contain a γ-stereogenic center.[17,18] This method was appealing because it would provide dhML (as the Boc methyl ester) in only two steps from the inexpensive chiral building block, Boc-(*S*)-serine-OMe.[17] After extensive optimization aimed at improving S_N2' vs. S_N2 selectivity and conversion (Extended Data Fig. 1), we obtained Boc-dhML-OMe **3** in 43% isolated yield (1.6 g) through the use of 50 mol% CuBr·DMS and 2 equivalents of crotyl chloride (Figure 2a). Boc to Fmoc exchange, followed by ester hydrolysis, provided Fmoc-dhML **5**, which was incorporated into the linear heptapeptide as described below.

A solid-phase route was previously employed to synthesize a linear heptapeptide precursor of ternatin, followed by solution-phase cyclization.[14] However, this strategy involved macrocyclization between the secondary amine of *N*-Me-Ala7 and the carboxylic acid of

Author Manuscript Author Manuscript Author Manuscript Author Manuscript

Leu1 (Figure 2b, site A), which we found to be low yielding in the context of peptides containing dhML.[15] Thus, we sought to identify an alternative cyclization site using the ternatin-related cyclic peptide **6** as a model system (Figure 2c). Linear heptapeptide precursors were synthesized on the solid phase, deprotected and cleaved from the resin, and cyclized in solution (see Supplementary Information for details). Gratifyingly, cyclization at site B provided **6** in 63% overall yield (including the solid-phase linear heptapeptide synthesis), whereas cyclization at site A was less efficient (46% overall yield). By synthesizing the linear heptapeptide precursor on the solid phase and cyclizing in solution at site B, we were able to prepare ternatin-4 in 3 days and 70% overall yield (27 mg), a significant improvement over our previous route (Figure 2c). Most importantly, by incorporating Fmoc-protected (*S,R*)- and (*S,S*)-*N*-Me-β-OH-Leu, we completed the first total syntheses of SR-A3 (21 mg, 35% overall yield) and SS-A3 (5 mg, 21% overall yield).

Synthetic SR-A3 is indistinguishable from naturally derived A3

With synthetic SR-A3 and SS-A3 in hand (Figure 3a), we first compared their HPLC elution profiles with an authentic sample of the Aspergillus-derived natural product A3. SR-A3 and naturally derived A3 had identical retention times, whereas SS-A3 eluted later in the gradient (Figure 3b). Furthermore, the ^{1}H and ^{13}C NMR spectra of SR-A3 were identical to the corresponding spectra of natural A3 (Figure 3c). Finally, SR-A3 and naturally derived A3 blocked proliferation of HCT116 cancer cells with superimposable dose-response curves (Figure 3d, IC_{50} ~0.9 nM), whereas SS-A3 was ~3-fold less potent (IC_{50} ~2.7 nM). Similar trends were observed in four additional cancer cell lines (Extended Data Fig. 2). Together, these data are consistent with our stereochemical hypothesis and strongly suggest that synthetic SR-A3 and natural A3 have the same structure.

N-Me-β-OH-Leu stereospecifically confers increased cellular residence time

We previously demonstrated that ternatin-4 is inactive toward a human cancer cell line that is homozygous for an Ala399Val mutation in eEF1A (encoded by the *EEF1A1* gene).[15] These cells were also resistant to SR-A3 (IC_{50} >> 1 μM), providing strong genetic evidence that eEF1A is the relevant target (Figure 4a). Consistent with this interpretation, treatment of cells with SR-A3 for 24 h inhibited global protein synthesis with an IC_{50} of ~20 nM (Figure 4b), as measured by a clickable puromycin (*O*-propargyl puromycin, OPP) incorporation assay (Extended Data Fig. 3).[19] Under these conditions – 24 h of continuous treatment prior to a 1-h pulse with OPP –- SR-A3 behaved identically to ternatin-4, whereas SS-A3 was slightly less potent. Based on these cellular data, it remained unclear as to whether *N*-Me-β-OH-Leu in SR-A3 confers any advantage over the biosynthetically less ornate *N*-Me-Leu found in ternatin and ternatin-4.

Drug-target residence time, which reflects not only the biochemical off-rate, but also the rebinding rate and local target density in vivo, has emerged as a critical kinetic parameter in drug discovery.[20,21] To test for potential differences in cellular residence time, we treated HCT116 cells with 100 nM SR-A3, SS-A3, or ternatin-4 for 4 h, followed by washout into drug-free media. At various times post-washout, cells were pulse-labeled with OPP for 1 h. Whereas protein synthesis rates partially recovered in cells treated with ternatin-4 or SS-A3 (~30% of DMSO control levels, 24 h post-washout), transient exposure of cells to

Author Manuscript Author Manuscript Author Manuscript Author Manuscript

SR-A3 resulted in more prolonged inhibition (Figure 4c). To confirm the extended duration of action observed with SR-A3, we assessed cell proliferation during a 72-h washout period. Strikingly, cell proliferation over 72 h was sharply reduced after 4-h treatment with 100 nM SR-A3, followed by rigorous washout. By contrast, cell proliferation rates recovered nearly to DMSO control levels after transient exposure to 100 nM ternatin-4 or SS-A3 (Figure 4d). These results demonstrate that the (*R*)-β-hydroxy group attached to *N*-Me-Leu endows SR-A3 with a substantial kinetic advantage over SS-A3 and ternatin-4, as reflected by washout resistance and increased cellular residence time associated with inhibition of protein synthesis and cell proliferation.

smFRET imaging reveals enhanced residence time and rebinding kinetics of SR-A3

To gain mechanistic insight into SR-A3's kinetic advantage in cells relative to ternatin-4 and SS-A3, we employed smFRET imaging of biochemically reconstituted, eEF1A-catalyzed translation reactions.[22] In this assay, tRNA in the P site of surface-immobilized human ribosomes is labeled with a donor fluorophore (Cy3) (Figure 5a). Aminoacyl-tRNA (aa-tRNA) labeled with an acceptor fluorophore (LD655) is then stopped-flow delivered as a ternary complex (TC) with eEF1A and GTP. The resulting reaction is monitored in real time using a home-built total internal reflection microscope.[23] The FRET efficiency between the two fluorophores – inversely related to the distance between the two tRNAs – increases through a series of well-characterized states (Figure 5a): initiation complex (**IC**), GTPase-activated (**GA**), and fully accommodated (**AC**).[22,24]

Before TC addition, no FRET is observed (Figure 5a, **IC**; Figure 5b). When TC is introduced to the microscope flow cell, it binds rapidly to the ribosomal A site where codon-anticodon recognition occurs (Figure 5a, **GA**), resulting in GTP hydrolysis and subsequent dissociation of eEF1A from aa-tRNA and the ribosome. The ribosome complex exhibits similar time-averaged FRET efficiencies of ~0.5 at both GA states (before and immediately after eEF1A dissociation). Upon eEF1A dissociation, aa-tRNA accommodates into the ribosomal peptidyl transferase center (Figure 5a, **AC**), as revealed by the marked increase in FRET efficiency to ~0.7 in DMSO control reactions (Figure 5b, left). By contrast, when TC was delivered in the presence of 10 μM ternatin-4, SS-A3, or SR-A3, aa-tRNA accommodation was strongly inhibited, whereas formation of the initial TC/ribosome intermediate was unaffected (Figure 5b). These results suggest that all three compounds similarly stall elongating ribosomes bound to TC (Figure 5a, **GA**), presumably by preventing conformational changes in eEF1A (either before or after GTP hydrolysis), which are required for its dissociation from aa-tRNA and the ribosome.

Since SR-A3 exhibited greater cellular residence time than ternatin-4 or SS-A3 (Figure 4e), we designed a series of in vitro chase experiments to quantify differences in dissociation rates and rebinding constants between these closely related analogs. We first generated a population of drug-stalled elongation complexes by incubating immobilized ribosomes with TC and 10 μM of each drug for 30 seconds. Excess TC and drugs were then washed out of the microscope flow cell with buffer containing 0, 2.5, 5, 7.5, or 10 μM drug at the start of data acquisition. Under these washout conditions, drug-stalled elongation complexes can gradually transition into the fully accommodated high-FRET state (Figure 5c, example

Author Manuscript Author Manuscript Author Manuscript Author Manuscript

trace showing washout into drug-free buffer). We estimated the average time required for aa-tRNA accommodation to occur in each washout condition (t_{acc}) from cumulative dwell-time distributions by calculating the fraction of ribosomes that reached the high-FRET state at each time point and fitting exponential functions to the resulting data (Figure 5d and Extended Data Fig. 4a, see Methods for details).

Given the assumption that drug dissociation must occur prior to aa-tRNA accommodation, the drug residence times and rebinding constants can then be determined from the chase series (Figure 5e, see Methods for details).[25,26] Based on the measured inhibition time after washout into drug-free buffer, the residence time of SR-A3 (82 s) is about 60% longer than ternatin-4 (56 s) or SS-A3 (51 s). In addition, the rebinding constant, which corresponds to the drug concentration in the washout buffer required to double the inhibition time (relative to drug-free buffer) through drug rebinding events, strongly favors SR-A3 (Figure 5e). This implies that SR-A3 rebinds to the stalled eEF1A-ribosome complex (**GA** or related states, Figure 5a) twice as fast as SS-A3 and four times as fast as ternatin-4 (Figure 5e and Extended Data Fig. 4b). Taken together, and consistent with our cell-based findings, our smFRET data show that (*S,R*)-*N*-Me-β-OH-Leu stereospecifically endows SR-A3 with a longer residence time and faster target rebinding kinetics upon dissociation.

SR-A3 treatment significantly extends survival of Eμ-Myc tumor-bearing mice

The oncogenic transcription factor Myc is dysregulated in >50% of human cancers.[27] Structural alterations of the *MYC* gene cause B-cell lymphoma in humans and mice,[28–31] and a Myc-dependent increase in protein synthesis is a key oncogenic determinant.[32] The Eμ-Myc transgenic mouse,[28] in which Myc is specifically overexpressed in B lymphocytes, has been employed as a preclinical model of human Burkitt lymphoma and other Myc-driven B-cell malignancies. Hence, the Eμ-Myc model is a paradigm for testing whether inhibition of protein synthesis downstream of Myc oncogenic activity confers therapeutic benefit. Given its enhanced residence time and rebinding kinetics, as well as improved metabolic stability (Extended Data Fig. 5a), we selected SR-A3 for a preclinical trial using the Eμ-Myc lymphoma allograft model. After intravenous injection of wild-type immunocompetent mice with mouse Eμ–Myc/+ lymphoma cells and waiting until tumors were palpable (~2 weeks after injection), we began treatment with either vehicle or SR-A3 (dosed 3 times per week, 1.5 or 2.0 mg/kg, by intraperitoneal injection). Treatment of tumor-bearing mice with single-agent SR-A3 dramatically prolonged survival in a dose-dependent manner (Figure 6a). Moreover, SR-A3 was well tolerated in both dose groups, and no significant body weight loss was observed (Extended Data Fig. 5b).

Having established an efficacious and well-tolerated dosing regimen for SR-A3, we sought to test whether its enhanced residence time relative to ternatin-4 translates to improved antitumour activity in vivo. To ensure a fair comparison in the head-to-head antitumour study, we first assessed the pharmacokinetics of each compound in mice (2 mg/kg, single intraperitoneal injection). The area under the plasma concentration-time curve (AUC_{inf}) for SR-A3 was ~2.1-fold higher than ternatin-4 (Figure 6b), and the maximum plasma concentration (C_{max}) was ~1.7-fold higher (Extended Data Fig. 6a). We therefore treated Eμ-Myc tumor-bearing mice with either vehicle, 4.2 mg/kg ternatin-4, or 2 mg/kg SR-A3 (3

Author Manuscript Author Manuscript Author Manuscript Author Manuscript

times per week, n = 5 mice per treatment arm). After two weeks of treatment, tumors from each mouse were collected and weighed. Strikingly, SR-A3 treatment significantly reduced tumor burden, whereas ternatin-4 had no significant effect (Figure 6c and Extended Data Fig. 6b,c). These results demonstrate the clear improvement in antitumour efficacy conferred by (*R*)-β-OH-*N*-Me-Leu and suggest that SR-A3 may be a viable preclinical candidate for the treatment of Myc-driven B lymphoid tumors.

Discussion

In this study, we first developed an improved synthetic route to dhML-containing ternatin variants, culminating in the first total syntheses of SR-A3 and SS-A3 (Figure 2). Our work provides spectroscopic, chromatographic, and pharmacological evidence that synthetic SR-A3 (and not SS-A3) is identical to the fungal natural product "A3" (Figure 3), confirming the previous partial structure elucidation and providing the first complete stereochemical assignment of this potent eEF1A antagonist.

SR-A3 differs structurally from the previously reported eEF1A inhibitor, ternatin-4, by the addition of a single oxygen atom into the side chain of *N*-Me-Leu (Figure 1). We speculate that A3 is evolutionarily related to ternatin via acquisition of biosynthetic modules for (*R*)-pipecolic acid and (*S*,*R*)-dhML, as well as stereospecific hydroxylation of *N*-Me-Leu by the A3-producing fungus. Although amino acid β-hydroxylation is a common biosynthetic modification in cyclic peptide natural products, its stereospecific functions are mostly unknown. An unexpected finding from our work is that the *N*-Me-Leu β-hydroxyl in SR-A3 has little effect on cellular potency under continuous treatment conditions, as compared with ternatin-4. Rather, the β-hydroxyl in SR-A3, but not SS-A3, confers a dramatic increase in drug-target residence time and rebinding kinetics, as revealed by washout experiments in cells and reconstituted eEF1A-catalyzed elongation reactions monitored by smFRET (Figure 4c,d and Figure 5). We note that "drug-target residence time" measured in cells and tissues is determined by both drug dissociation and rebinding kinetics. Moreover, the intracellular concentration (or local density) of the target can play a major role in drug rebinding kinetics.[20] This can potentially explain the much longer residence time in cells, where [eEF1A] is ~35 μM,[33] as compared to the smFRET flow cell, where [eEF1A] is <<10 nM post-washout. The structural basis of SR-A3's enhanced binding kinetics will likely require cryo-electron microscopy analysis of stalled SR-A3/eEF1A/ribosome complexes at atomic resolution. Although the precise molecular mechanism by which the β-hydroxyl confers this kinetic advantage awaits further investigation, our study nevertheless reveals the power of smFRET imaging to illuminate differences in drug dissociation and rebinding kinetics, both of which can contribute to drug-target residence time and therapeutic efficacy.[20]

Dysregulation of the transcription factor Myc underlies multiple human cancers.[27] Nevertheless, Myc is still considered "undruggable" and no direct Myc inhibitors have advanced into clinical trials. Because the oncogenic activity of Myc relies on its ability to promote ribosome biogenesis and protein synthesis, an alternative approach is to attenuate protein synthesis rates. The Eμ-Myc lymphoma model has been employed to test various protein synthesis inhibition strategies, often in combination with other cytotoxic drugs. Targeting the protein synthesis machinery in Eμ-Myc mice either genetically[32] or

Author Manuscript Author Manuscript Author Manuscript Author Manuscript

pharmacologically[34–36] has been shown to suppress tumor growth and prolong overall survival. However, to the best of our knowledge, no translation elongation inhibitors have shown single-agent efficacy in this aggressive B-cell lymphoma model.

Our preclinical trial revealed that intermittent, low doses of SR-A3 (1.5–2.0 mg/kg, three times per week), but not the des-OH variant ternatin-4, profoundly reduced tumor burden and extended the survival of Eμ-Myc mice without obvious toxicity (Figure 6). SR-A3 thus shows therapeutic potential for the treatment of Myc-driven B-cell lymphoma. Our study of SR-A3 chemistry and biology provides a compelling illustration of how a “ligand efficient” side-chain modification (one oxygen atom) can be exploited to alter the pharmacological properties and residence time of a cyclic peptide natural product.

Methods

Cell culture

HCT116 cells (ATCC, Manassas, VA) were maintained in McCoy’s 5A media (Gibco, Grand Island, NY) supplemented with 10% fetal bovine serum (Axenia Biologix, Dixon, CA), 100 units/mL penicillin, and 100 μg/mL streptomycin (Gibco). H929 cells (ATCC) were maintained in advanced RPMI 1640 media (Gibco) supplemented with 6% fetal bovine serum, 2 mM glutamine, 100 units/mL penicillin, and 100 mg/mL streptomycin. MM1S, Jurkat, and Ramos cells (ATCC) were maintained in RPMI 1640 media (Gibco) supplemented with 10% fetal bovine serum, 100 units/mL penicillin, and 100 mg/mL streptomycin. All cells were cultured at 37°C in a 5% CO_2 atmosphere.

The natural product A3 was purified as described previously.[13]

Proliferation assay

Adherent cells were briefly trypsinized and repeatedly pipetted to produce a homogeneous cell suspension. 2,500 cells were seeded in 100 μL complete growth media per well in 96-well clear-bottom plates. Suspension cells were repeatedly pipetted to produce a homogenous cell suspension. 10,000 cells were seeded in 100 μL complete growth media per well in 96-well clear-bottom plates. After allowing cells to grow/adhere overnight, cells were treated with 25 μL/well 5x drug stocks (0.1% DMSO final) and incubated for 72 hours. AlamarBlue (Life Technologies, Grand Island, NY) was used to assess cell viability per the manufacturer’s instructions. Briefly, 12.5 μL alamarBlue reagent was added to each well, and plates were incubated at 37°C. Fluorescence intensity was measured every 30 min to determine the linear range for each assay (Ex 545 nm, Em 590 nm, SPARK, Tecan Austria GmbH, Austria). Proliferation curves were generated by first normalizing fluorescence intensity in each well to the DMSO-treated plate average. Normalized fluorescence intensity was plotted in GraphPad Prism (GraphPad, La Jolla, CA), and IC_{50} values were calculated from nonlinear regression curves. The reported IC_{50} values represent the average of at least three independent determinations (± SD).

Author Manuscript Author Manuscript Author Manuscript Author Manuscript

Washout-proliferation assay

Adherent cells were briefly trypsinized and repeatedly pipetted to produce a homogenous cell suspension. 2,500 cells were seeded in 100 μL complete growth media per well in 96-well clear-bottom plates. After allowing cells to grow/adhere overnight, cells were treated with ternatin analogs (100 nM, 0.1% DMSO final) and incubated for the indicated times. Growth media was carefully removed, cells were washed with warm PBS twice (2x short wash), followed by 5 min incubation in warm media at 37°C (long wash). This "short-long" washing cycle was repeated 3 times. After indicated times post-washout, CellTiter Glo (Promega, Madison, WI) was used to assess cell viability per the manufacturer's instructions. Briefly, after adding 100 μL CellTiter Glo reagent to each well, the plate was rocked at room temperature for 5–10 min, and the luminescence intensity was measured. Proliferation curves were generated by first normalizing luminescence intensity in each well to the average values from the t = 0 time point. Normalized luminescence intensity was plotted in GraphPad Prism (GraphPad, La Jolla, CA). The reported values represent the average of at least three independent determinations (± SD). Statistical significance was determined by one-way ANOVA followed by Sidak's multiple comparisons test.

OPP incorporation assay

HCT116 cells at 60% confluency in 12-well plates were incubated with the indicated concentrations of ternatin analogs for 10 min or 24 h at 37°C. After the indicated times, *O*-propargyl-puromycin (30 μM final concentration) was added, and the cells were incubated for 1 hour at 37°C. Subsequently, media was removed, and the cells were trypsinized, collected, and washed twice with ice-cold PBS before transferring to a 96-well V bottom plate. 100 μL Zombie Green (BioLegend, San Diego, CA) solution was added to each well and incubated for 30 min at RT in the dark. Cells were then washed with 2% FBS in PBS before fixation with 200 μL of 4% PFA in PBS for 15 min on ice in the dark. After washing the cells with 2% FBS in PBS, 200 μL permeabilization buffer (3% FBS, 0.1% saponin in PBS) was added to each well, and the cells were incubated for 5 min at RT in the dark. Cells were then washed and resuspended in 25 μL permeabilization buffer. 100 μL click chemistry mix (50 mM HEPES pH 7.5, 150 mM NaCl, 400 μM TCEP, 250 μM TBTA, 5 μM CF647-Azide (Biotium, Fremont, CA), 200 μM $CuSO_4$) was added to each well, and cells were incubated at RT in the dark. After overnight incubation, the cells were washed with permeabilization buffer followed by FACS buffer (2% FBS, 1% P/S, 2 mM EDTA, in PBS w/o Ca/Mg). Cells were then resuspended in 200 μL FACS buffer and filtered before FACS analysis (CytoFLEX, Beckman-Coulter, Brea, CA; FlowJo V10.7.1, BD, Franklin Lakes, NJ). Please see Supplementary Figure 1 for the gating strategy. Protein synthesis inhibition curves were generated by gating for single live cells and plotting mean fluorescence intensity (MFI) relative to the DMSO control values using GraphPad Prism (GraphPad, La Jolla, CA). IC_{50} values were calculated from nonlinear regression curves. The reported values represent the average of at least three independent determinations (± SD).

Author Manuscript Author Manuscript Author Manuscript Author Manuscript

Washout-OPP assay

HCT116 cells at 60% confluency in 12-well plates were incubated with compounds at 100 nM for 4 h at 37°C. Media was carefully removed, and cells were washed with warm PBS twice (2x short wash), followed by 5 min incubation in warm media at 37°C (long wash). After repeating the "short-long" washout cycle 3 times, cells were then resuspended in warm media and incubated at 37°C. After the indicated times post-washout, *O*-propargyl-puromycin (30 μM final concentration) was added, and the cells were incubated for an additional 1 h at 37°C. The media was removed, and the cells were trypsinized, collected, and washed twice with ice-cold PBS before transferring to a 96-well V bottom plate. 100 μL Zombie Green (BioLegend, San Diego, CA) solution was added to each well and incubated for 30 min at RT in the dark. Cells were then washed with 2% FBS in PBS before fixation with 200 μL of 4% PFA in PBS for 15 min on ice in the dark. After washing the cells with 2% FBS in PBS, 200 μL permeabilization buffer (3% FBS, 0.1% saponin in PBS) was added to each well, and cells were incubated for 5 min at RT in the dark. Cells were then washed and resuspended in 25 μL permeabilization buffer. 100 μL click chemistry mix (50 mM HEPES pH 7.5, 150 mM NaCl, 400 μM TCEP, 250 μM TBTA, 5 μM CF647-Azide (Biotium, Fremont, CA), 200 μM $CuSO_4$) was added to each well, and cells were incubated at RT in the dark. After the overnight incubation, cells were washed with permeabilization buffer followed by FACS buffer (2% FBS, 1% P/S, 2 mM EDTA, in PBS w/o Ca/Mg). Cells were then resuspended in 200 μL FACS buffer and filtered before FACS analysis as described above. Statistical significance was determined by one-way ANOVA followed by Sidak's multiple comparisons test.

smFRET data collection

Ribosomes from HEK293T cells, elongation factor eEF1A, and fluorescence-labeled tRNAs were prepared using the protocol described previously.[37] All smFRET experiments were carried out at 25 °C in human polymix buffer (20 mM HEPES pH 7.5, 5 mM $MgCl_2$, 140 mM KCl, 10 mM NH_4Cl, 2 mM spermidine, 5 mM putrescine and 1.5 mM 2-mercaptoethanol) containing 500 μM cycloheximide and a mixture of triplet-state quenchers (1 mM trolox, 1 mM 4-nitrobenzyl alcohol (NBA), 1 mM cyclooctatetraene (COT)) and an enzymatic oxygen scavenging system (2 μM 3,4-dihydroxybenzoic acid (PCA), 0.02 Units/ml protocatechuate *3,4*-dioxygenase (PCD)). The time-evolution of the FRET signal was recorded using a home-built total internal reflection-based fluorescence microscope at ~0.1 kW/cm^2 laser (532 nm) illumination. Movies were recorded either in time-lapse mode with one 500 ms frame acquired every 10 seconds or continuously at a time resolution of 500 ms. Donor and acceptor fluorescence intensities were extracted from the recorded movies and FRET efficiency traces were calculated using the SPARTAN software package.[23] FRET traces were selected for further analysis according to the following criteria: a single catastrophic photobleaching event, at least 8:1 signal/background-noise ratio and 6:1 signal/signal-noise ratio, less than four donor-fluorophore blinking events, and a correlation coefficient between donor and acceptor < 0.5. The resulting smFRET traces were analyzed using Hidden Markov model idealization methods as implemented in the SPARTAN software package.[23]

Author Manuscript Author Manuscript Author Manuscript Author Manuscript

Ternary complex real-time delivery experiments

80S initiation complexes containing Met-tRNA^{fMet}-Cy3 and displaying the codon UUC in the A site were immobilized on passivated quartz slides as described previously.[37,38] This was followed by delivery of 10 nM eEF1A ternary complex containing Phe-tRNA^{Phe}-LD655 together with 1 mM GTP and either DMSO or 10 μM drug at the start of data acquisition.

Drug chase experiments

Stalled pre-accommodation complexes were formed by immobilization of 80S initiation complexes containing Met-tRNA^{fMet}-Cy3 and displaying the codon UUC in the A site to passivated quartz slides as described previously[37,38] followed by delivery of 10 nM eEF1A ternary complex containing Phe-tRNA^{Phe}-LD655 together with 1 mM GTP and 10 μM drug. After 30 s of incubation, the chase was started by delivery of buffer containing either 0, 2.5, 5, 7.5, or 10 μM drug concurrent with the start of data acquisition.

smFRET data kinetic analysis

To construct cumulative distribution plots suitable for estimation of kinetic parameters, FRET traces were first idealized using Hidden Markov model analysis to a model with three FRET states (FRET efficiencies: −0.0043 ± 0.06, 0.4485 ± 0.06, and 0.7070 ± 0.06) and then the cumulative sum of molecules that had arrived at the highest (0.7070) FRET state in each movie frame was calculated. To estimate reaction mean times and their associated uncertainties, 1000 bootstrap samples were generated from each experimental replicate and mean times were estimated by fitting of single-exponential functions to these data (Equation 1), taking into account unobserved events due to photobleaching of the fluorophores or dissociation of the intact ternary complex from the ribosomal A site by multiplying the estimated mean time with the inverse of the fraction of traces were accommodation was observed at the end of the process.[25]

$$f_{acc}(t) = \left(1 - e^{\frac{-1}{\frac{1}{f_{acc}(\infty)}\tau_{acc}}t}\right) \quad \text{Equation 1}$$

Mean rates and standard errors were calculated as the weighted averages of two to three experimental replicates for each drug concentration. For estimation of drug residence times and rebinding constants these estimated mean times were plotted against drug concentration and Equation 2 was fitted to the data.[25,26]

$$\tau_I([Drug]) = \tau_0\left(1 + \frac{[Drug]}{K_I}\right) \quad \text{Equation 2}$$

In Equation 2, τ_I is the observed inhibition mean time as a function of drug concentration. τ_0 is the drug residence time each time it binds, and K_I is the rebinding constant corresponding to the drug concentration required to double the inhibition time through drug rebinding events, it can be interpreted as the ratio between the drug association rate constant and the rate of the process that renders the ribosome immune to drug inhibition, in this case conformational changes in eEF1A.

Author Manuscript Author Manuscript Author Manuscript Author Manuscript

Animal Experiments

All animal experiments were approved by The University of California San Francisco Institutional Animal Care and Use Committee (UCSF-IACUC). *Eμ-Myc/+* transgenic mice were purchased from the Jackson Laboratory (stock no. 002728). Primers used for genotyping are: 5'-CCG AGG TGA GTG TGA GAG G-3'; 5'-AAA CAG TAA TAG CGC AGC A-3'. For *Eμ-Myc* clonal B-cell line collection, *Eμ-Myc/+* mice harboring lymphoma were euthanized according to IACUC guidelines. Lymph nodes were collected immediately on ice, minced, and passed through a 40-μm cell strainer in cold PBS with 2% FBS. Cells were centrifuged at 300 *g* for 5 min. Cells were then resuspended in cold erythrocyte lysis solution ACK (Thermo Fisher A1049201) for 1 min. Isolated lymphoma cells were centrifuged at 300 *g* for 5 min and washed in PBS before freezing in cell cryopreservation medium and storing in liquid nitrogen. For the lymphoma preclinical trial, *Eμ-Myc/+* lymphoma cells were thawed and washed once in PBS. One million cells were injected intravenously into eight-week-old male C57BL/6 mice. Mice were monitored for lymphoma development by palpation every other day. Once the lymphoma tumors became palpable (~2 weeks after tumor cell injection), mice (5 per group) were dosed by intraperitoneal injection with either SR-A3 or vehicle (10% EtOH/Kolliphor EL in water) three times per week (every other day) until the survival end point (moribund mice were sacrificed; statistical significance of Kaplan-Meier survival curves was determined by logrank test), or for two weeks, at which time the tumors were dissected and weighed (statistical significance was determined by one-way ANOVA). The maximum allowable tumor size (2 cm in diameter) was not exceeded in any study. No animals or data points were excluded from the analyses.

Chemical synthesis (general)

All reactions in non-aqueous media were conducted under a positive pressure of dry argon in glassware that had been dried in oven prior to use, unless noted otherwise. Anhydrous solutions of reaction mixtures were transferred via an oven-dried syringe or cannula. All solvents were dried prior to use unless noted otherwise. Thin layer chromatography was performed using precoated silica gel plates (EMD Chemical Inc. 60, F254). Flash column chromatography was performed on CombiFlash Rf 200i system (Teledyne Isco, Lincoln, NE). ^{1}H and ^{13}C nuclear magnetic resonance spectra (NMR) were obtained on a Varian (Palo Alto, CA) Inova 400 MHz spectrometer recorded in ppm (δ) downfield of TMS (δ = 0) in $CDCl_3$ unless noted otherwise. NMR spectra were analyzed using MestReNova V14.1.1 (Mestrelab Research, Spain). Signal splitting patterns were described as singlet (s), doublet (d), triplet (t), quartet (q), quintet (quint), or multiplet (m), with coupling constants (*J*) in hertz. High resolution mass spectra (HRMS) were performed on Waters Xevo G2-XS QToF LC-MS system, eluting with a water/MeCN (+0.1% formic acid) gradient at 0.6 mL/min. Please see Supplementary Information for more details.

Data availability

Data supporting the findings of this study are available within the article and the Supplementary Information. Source data are provided with this paper.

Author Manuscript Author Manuscript Author Manuscript Author Manuscript

Statistics & Reproducibility

The statistical significance of the difference between experimental groups was determined by one-way analysis of variance (ANOVA), followed by Sidak's multiple comparisons test. P values indicate statistical significance denoted by *P < 0.05, **P < 0.01, ***P < 0.005, ****P < 0.0001, and not significant by P > 0.05. Data were organized using Microsoft Excel 2017, and graphing and statistical analyses were performed using Prism 8.4.0. All biological experiments (except Fig. 6D) were repeated at least twice with similar results. The experiment in Fig. 6D was performed once with 5 mice allocated to each dose group. Descriptions of the error bars and the number of replicates within each experiment are provided in the figure legends.

Extended Data

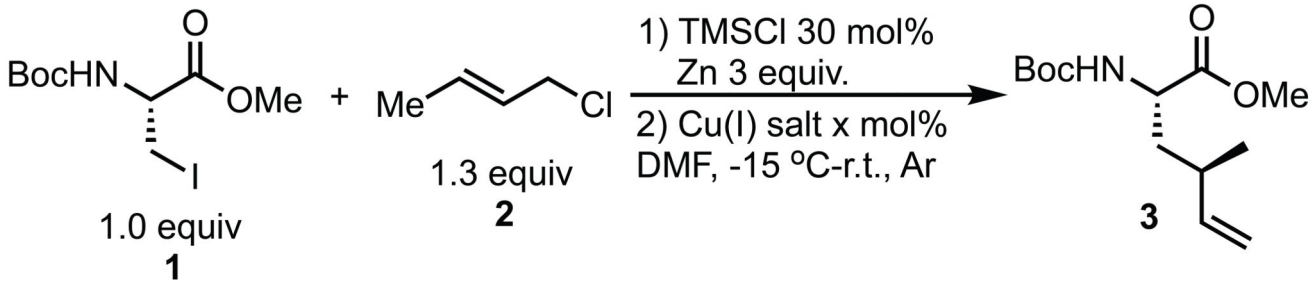

Entry	Cu(I) Salt	x	S_N2':S_N2 [a]	d.r. of S_N2' [a]	Yield [b]
1	CuBr·DMS	10	1.2:1	1:1	12%
2	CuBr·DMS	50	1.9:1	1.4:1	26%
3	CuBr·DMS	100	2.1:1	1.4:1	-
4	CuBr	100	1:3.5	-	-
5	CuCl	100	1:2.5	-	-
6	CuTC	100	-	-	N.R.
7[c]	CuBr·DMS	50	1:2.6	-	-
8[d]	**CuBr·DMS**	**50**	**1.8:1**	**1.4:1**	**43%**

[a] Ratio was based on the crude NMR of the reaction; [b] Isolated yield of **3**; [c] Crotyl bromide was used instead of **2**; [d] 2 equiv of crotyl chloride were used. DMS: dimethyl sulfide; TC: thiophene -2-carboxylate; N.R.: no reaction.

Extended Data Fig. 1. Screening conditions for Cu(I)-promoted S_N2' reaction.

Author Manuscript Author Manuscript Author Manuscript Author Manuscript

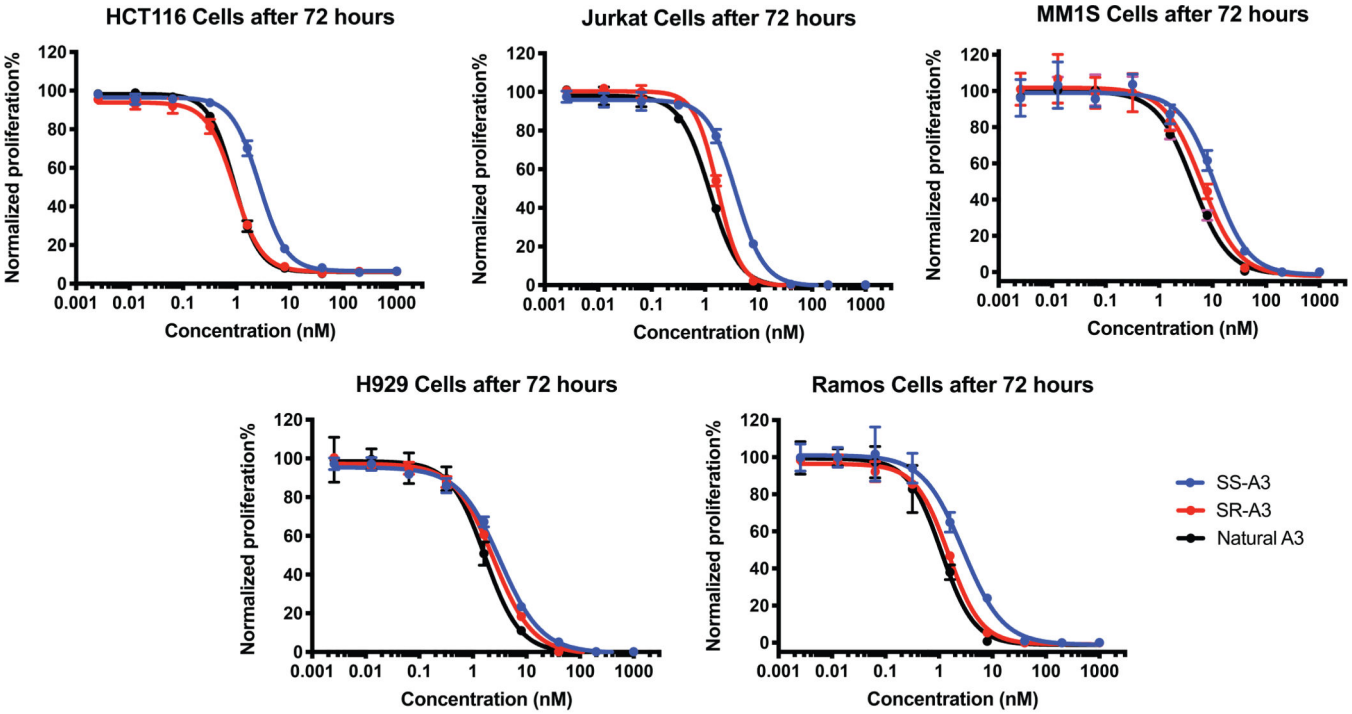

IC_{50} (nM)

	SS-A3	SR-A3	Natural A3
HCT116	2.67	0.92	0.91
Jurkat	3.78	1.71	1.22
MM1S	11.05	6.21	4.28
H929	3.20	2.43	1.69
Ramos	2.82	1.50	1.11

Extended Data Fig. 2. Effects on cancer cell proliferation.

The indicated cell lines were treated with DMSO or increasing concentrations of synthetic SR-A3 and SS-A3 and natural A3. After 72 h, cell proliferation was quantified using alamarBlue (% DMSO control, mean ± SD, n = 3). GraphPad Prism was used to calculate IC50 values.

Author Manuscript Author Manuscript Author Manuscript Author Manuscript

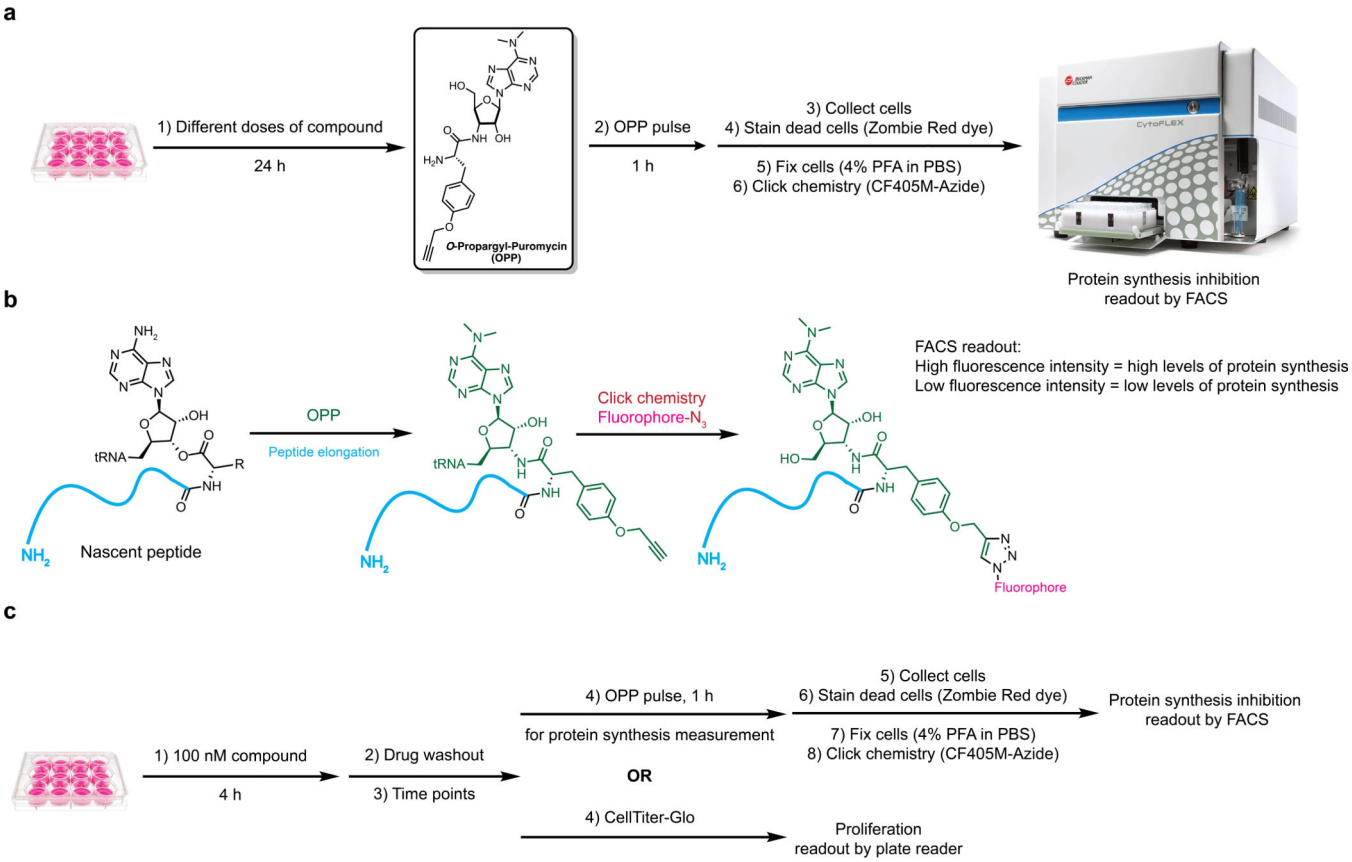

Extended Data Fig. 3. Measuring effects on cellular protein synthesis rates.

(**a**) General workflow for measuring protein synthesis rates in cells using *O*-Propargyl-Puromycin (OPP). See "OPP incorporation assay" in the methods section for details. (**b**) OPP is an aminoacyl-tRNA mimic (clickable puromycin derivative) that, like puromycin itself, is incorporated into ribosome-associated nascent polypeptides by reacting with peptidyl-tRNAs in the ribosomal P site. After fixing and permeabilizing cells, click chemistry is used to conjugate the OPP alkyne with a fluorophore azide, and the intracellular fluorescence intensity (proportional to the amount of actively translating ribosomes) is measured by flow cytometry. (**c**) General workflow for washout-OPP and washout-proliferation experiments.

Author Manuscript Author Manuscript Author Manuscript Author Manuscript

a

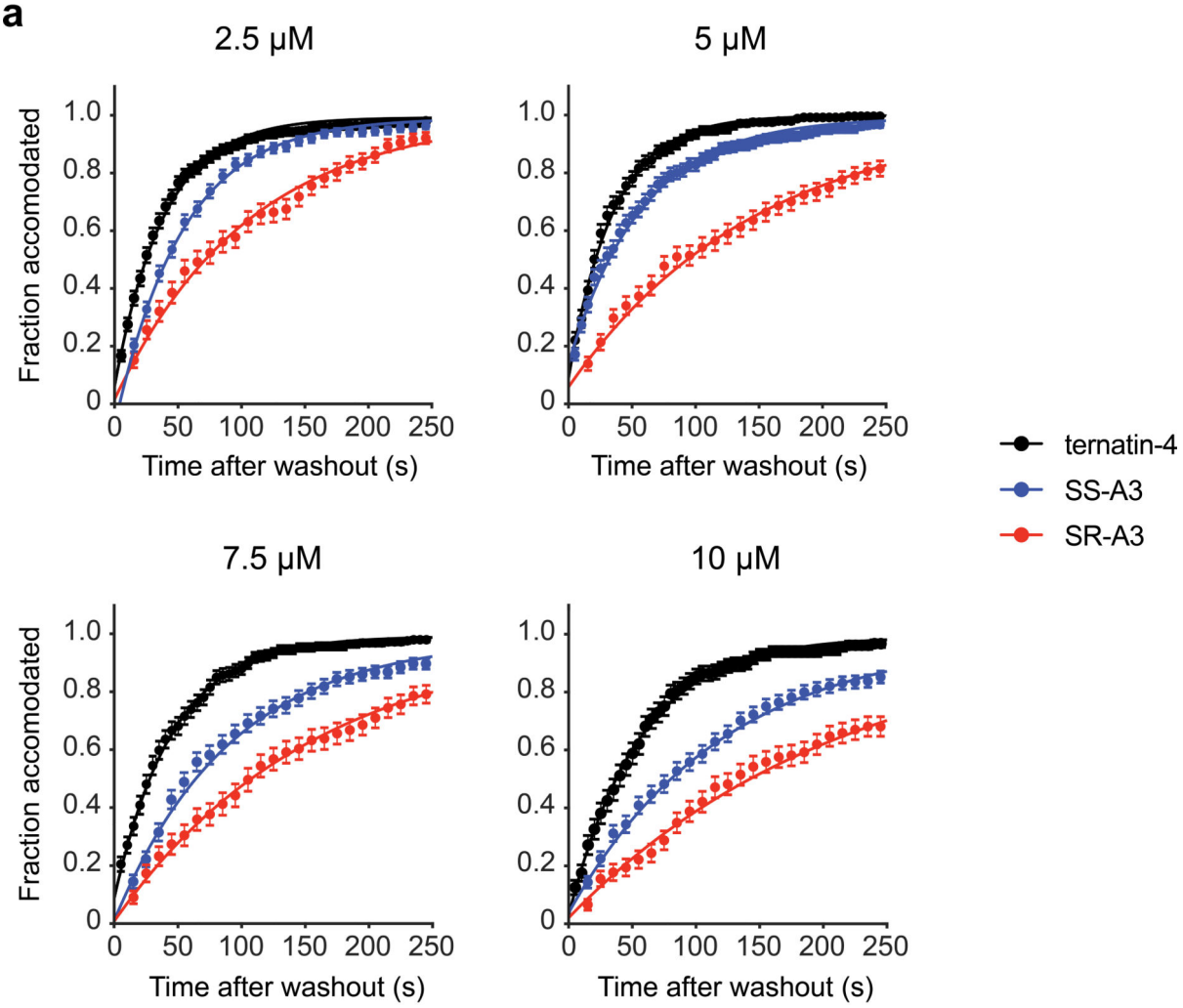

b

	Residence Time (s)	Inhibition Constant (μM)
ternatin-4	56 ± 4	10.4 ± 1.9
SS-A3	51 ± 2.5	5 ± 0.4
SR-A3	82 ± 1	2.67 ± 0.05

Extended Data Fig. 4. Time and concentration-dependent effects on aa-tRNA accommodation revealed by smFRET.

(**a**) Cumulative dissociation time distributions for ternatin-4, SS-A3, and SR-A3 at the indicated concentrations. Distributions are constructed as described in the main text and the methods. Error bars represent SEM derived from 1000 bootstrap replicates. (**b**) Tabulated kinetic parameters based on data in Figure 5 and Extended Data Fig. 4a.

Author Manuscript Author Manuscript Author Manuscript Author Manuscript

a

	Human Liver Microsome (remaining%)	Mouse Liver Microsome (remaining%)
ternatin-4	1.6%	1.2%
SS-A3	6.7%	7.4%
SR-A3	39.9%	31.8%

b

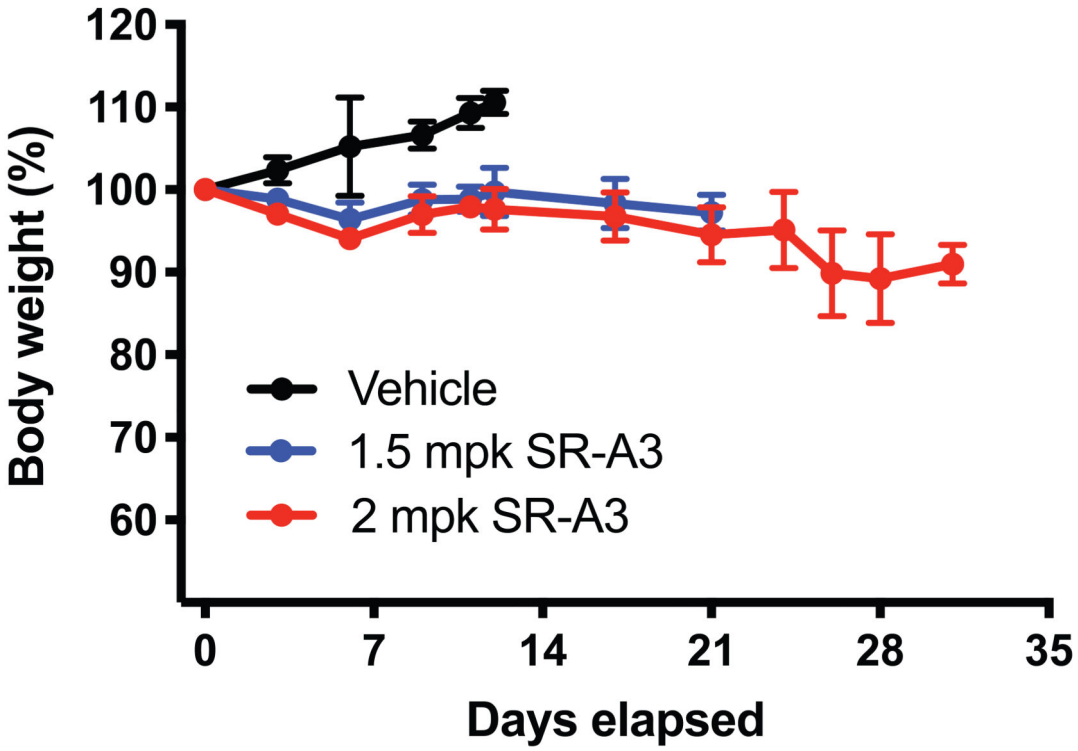

Extended Data Fig. 5. Microsome stability and effects on mouse body weight.

(**a**) Human and mouse liver microsome stability results. Percent remaining of each analog was quantified by LC/MS after incubating at 1 μM in the presence of human or mouse liver microsomes (with NADPH) for 30 min at 37°C. This study was performed by the contract research organization, Bioduro-Sundia (San Diego, CA). (**b**) Average body weight (± SD, relative to day 0) during the efficacy study in Eμ-Myc mice (n = 5 per arm, Figure 6a). Day 0 indicates the beginning of treatment.

Author Manuscript Author Manuscript Author Manuscript Author Manuscript

a

	$t_{1/2}$ (h)	t_{max} (h)	C_{max} (ng/mL)	AUC_{Last} (h*ng/mL)	AUC_{Inf} (%)	AUC_{Extr} (%)	MRT_{Inf} (h)	AUC_{Inf}/D (h*kg*ng/mL/mg)
ternatin-4	5.16	0.250	51.3	151	186	19.4	6.17	92.8
SR-A3	8.21	0.583	86.6	347	384	9.78	8.63	192

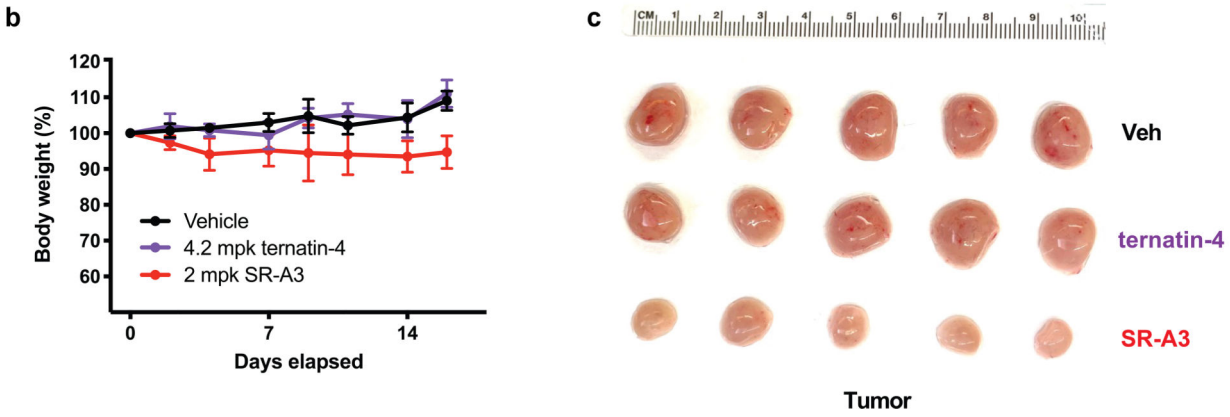

Extended Data Fig. 6. Pharmacokinetics and effects of ternatin-4 and SR-A3 on mouse body weight and tumor size.

(**a**) Mean pharmacokinetic (PK) parameters of ternatin-4 and SR-A3. Mice (n = 3) were intraperitoneally injected with ternatin-4 or SR-A3 (2 mg/kg), and plasma concentrations were quantified at various time points (Figure 6b). PK data were acquired and analyzed by the contract research organization, Bioduro-Sundia (San Diego, CA). (**b**) Average mouse body weight (± SD, relative to day 0) during the Eμ-Myc tumor study (Figure 6c). Day 0 indicates the beginning of treatment (n = 5 per arm). (**c**) Photographs of tumors from each mouse after two weeks of treatment (n =5 per arm).

Supplementary Material

Refer to Web version on PubMed Central for supplementary material.

Acknowledgments

Funding for this study was provided by the UCSF Program for Breakthrough Biomedical Research (J.T. and D.R.), the UCSF Invent Fund (J.T. and D.R.), the National Institutes of Health (5R01GM079238 to S.C.B. and R35CA242986 to D.R.), the American Cancer Society (American Cancer Society Research Professor Award to D.R.), and the Tobacco-Related Disease Research Program Postdoctoral Fellowship Awards (28FT-0014 to H.Y.W.). Part of this work was supported by Taylor's University PhD Scholarship program (A.A.Q.A.K.), as well as a research grant from the Ministry of Education of Malaysia FRGS [600-IRMI/FRGS 5/3 (011/2017) to J.F.W.].

References

1. Lin J, Zhou D, Steitz TA, Polikanov YS & Gagnon MG Ribosome-Targeting Antibiotics: Modes of Action, Mechanisms of Resistance, and Implications for Drug Design. Annu. Rev. Biochem 87, 451–478 (2018). [PubMed: 29570352]
2. Xu Y. & Ruggero D. The Role of Translation Control in Tumorigenesis and Its Therapeutic Implications. Annu. Rev. Cancer Biol 4, 437–457 (2020).
3. Fan A. & Sharp PP Inhibitors of Eukaryotic Translational Machinery as Therapeutic Agents. J. Med. Chem 64, 2436–2465 (2021). [PubMed: 33592144]

Author Manuscript Author Manuscript Author Manuscript Author Manuscript

4. Schuller AP & Green R. Roadblocks and resolutions in eukaryotic translation. Nat. Rev. Mol. Cell Biol 19, 526–541 (2018). [PubMed: 29760421]
5. Abbas W, Kumar A. & Herbein G. The eEF1A Proteins: At the Crossroads of Oncogenesis, Apoptosis, and Viral Infections. Front. Oncol 5, 75 (2015). [PubMed: 25905039]
6. Crews CM, Collins JL, Lane WS, Snapper ML & Schreiber SL GTP-dependent binding of the antiproliferative agent didemnin to elongation factor 1 alpha. J. Biol. Chem 269, 15411–15414 (1994). [PubMed: 8195179]
7. Shao S. et al. Decoding Mammalian Ribosome-mRNA States by Translational GTPase Complexes. Cell 167, 1229–1240.e1215 (2016). [PubMed: 27863242]
8. Lindqvist L. et al. Inhibition of translation by cytotrienin A--a member of the ansamycin family. RNA 16, 2404–2413 (2010). [PubMed: 20943818]
9. Krastel P. et al. Nannocystin A: an Elongation Factor 1 Inhibitor from Myxobacteria with Differential Anti-Cancer Properties. Angew. Chem. Int. Ed 54, 10149–10154 (2015).
10. Klein VG et al. Identifying the Cellular Target of Cordyheptapeptide A and Synthetic Derivatives. ACS Chem. Biol 16, 1354–1364 (2021). [PubMed: 34251165]
11. Spicka I. et al. Randomized phase III study (ADMYRE) of plitidepsin in combination with dexamethasone vs. dexamethasone alone in patients with relapsed/refractory multiple myeloma. Ann Hematol. 98, 2139–2150 (2019). [PubMed: 31240472]
12. White KM et al. Plitidepsin has potent preclinical efficacy against SARS-CoV-2 by targeting the host protein eEF1A. Science 371, 926–931 (2021). [PubMed: 33495306]
13. Blunt J. et al. Bioactive compounds. International Patent WO 2010/062159 A1.
14. Shimokawa K. et al. (−)-Ternatin, a highly N-methylated cyclic heptapeptide that inhibits fat accumulation: structure and synthesis. Tetrahedron Lett. 47, 4445–4448 (2006).
15. Carelli JD et al. Ternatin and improved synthetic variants kill cancer cells by targeting the elongation factor-1A ternary complex. Elife 4, e10222 (2015).
16. Gordon DE et al. A SARS-CoV-2 protein interaction map reveals targets for drug repurposing. Nature 583, 459–468 (2020). [PubMed: 32353859]
17. Deboves HJC, Grabowska U, Rizzo A. & Jackson RFW A new route to hydrophobic amino acids using copper-promoted reactions of serine-derived organozinc reagents. J. Chem. Soc., Perkin Trans 1 2000, 4284–4292 (2000).
18. Dunn MJ, Jackson RFW, Pietruszka J. & Turner D. Synthesis of Enantiomerically Pure Unsaturated alpha-Amino Acids Using Serine-Derived Zinc/Copper Reagents. J. Org. Chem 60, 2210–2215 (1995).
19. Liu J, Xu Y, Stoleru D. & Salic A. Imaging protein synthesis in cells and tissues with an alkyne analog of puromycin. Proc. Natl. Acad. Sci. U.S.A 109, 413–418 (2012). [PubMed: 22160674]
20. Vauquelin G. Rebinding: or why drugs may act longer in vivo than expected from their in vitro target residence time. Expert Opin. Drug Discov 5, 927–941 (2010). [PubMed: 22823988]
21. Copeland RA The drug-target residence time model: a 10-year retrospective. Nat. Rev. Drug Discov 15, 87–95 (2016). [PubMed: 26678621]
22. Ferguson A. et al. Functional Dynamics within the Human Ribosome Regulate the Rate of Active Protein Synthesis. Mol. Cell 60, 475–486 (2015). [PubMed: 26593721]
23. Juette MF et al. Single-molecule imaging of non-equilibrium molecular ensembles on the millisecond timescale. Nat. Methods 13, 341–344 (2016). [PubMed: 26878382]
24. Geggier P. et al. Conformational sampling of aminoacyl-tRNA during selection on the bacterial ribosome. J. Mol. Biol 399, 576–595 (2010). [PubMed: 20434456]
25. Borg A. et al. Fusidic acid targets elongation factor G in several stages of translocation on the bacterial ribosome. J. Biol. Chem 290, 3440–3454 (2015). [PubMed: 25451927]
26. Holm M, Borg A, Ehrenberg M. & Sanyal S. Molecular mechanism of viomycin inhibition of peptide elongation in bacteria. Proc. Natl. Acad. Sci. U.S.A 113, 978–983 (2016). [PubMed: 26755601]
27. Gabay M, Li Y. & Felsher DW MYC activation is a hallmark of cancer initiation and maintenance. Cold Spring Harb. Perspect. Med 4, a014241 (2014).

Author Manuscript Author Manuscript Author Manuscript Author Manuscript

28. Harris AW et al. The E mu-myc transgenic mouse. A model for high-incidence spontaneous lymphoma and leukemia of early B cells. J. Exp. Med 167, 353–371 (1988). [PubMed: 3258007]
29. Gelmann EP, Psallidopoulos MC, Papas TS & Dalla-Favera R. Identification of reciprocal translocation sites within the c-myc oncogene and immunoglobulin mu locus in a Burkitt lymphoma. Nature 306, 799–803 (1983). [PubMed: 6419123]
30. Reddy A. et al. Genetic and Functional Drivers of Diffuse Large B Cell Lymphoma. Cell 171, 481–494.e415 (2017). [PubMed: 28985567]
31. Chapuy B. et al. Molecular subtypes of diffuse large B cell lymphoma are associated with distinct pathogenic mechanisms and outcomes. Nat. Med 24, 679–690 (2018). [PubMed: 29713087]
32. Barna M. et al. Suppression of Myc oncogenic activity by ribosomal protein haploinsufficiency. Nature 456, 971–975 (2008). [PubMed: 19011615]
33. Itzhak DN, Tyanova S, Cox J. & Borner GH Global, quantitative and dynamic mapping of protein subcellular localization. Elife 5, e16950 (2016).
34. Pourdehnad M. et al. Myc and mTOR converge on a common node in protein synthesis control that confers synthetic lethality in Myc-driven cancers. Proc. Natl. Acad. Sci. U.S.A 110, 11988–11993 (2013). [PubMed: 23803853]
35. Robert F. et al. Altering chemosensitivity by modulating translation elongation. PLOS ONE 4, e5428 (2009).
36. Bordeleau ME et al. Therapeutic suppression of translation initiation modulates chemosensitivity in a mouse lymphoma model. J. Clin. Investig 118, 2651–2660 (2008). [PubMed: 18551192]
37. Flis J. et al. tRNA Translocation by the Eukaryotic 80S Ribosome and the Impact of GTP Hydrolysis. Cell Rep. 25, 2676–2688.e2677 (2018). [PubMed: 30517857]
38. Blanchard SC, Kim HD, Gonzalez RL Jr., Puglisi JD & Chu S. tRNA dynamics on the ribosome during translation. Proc. Natl. Acad. Sci. U.S.A 101, 12893–12898 (2004). [PubMed: 15317937]

Author Manuscript Author Manuscript Author Manuscript Author Manuscript

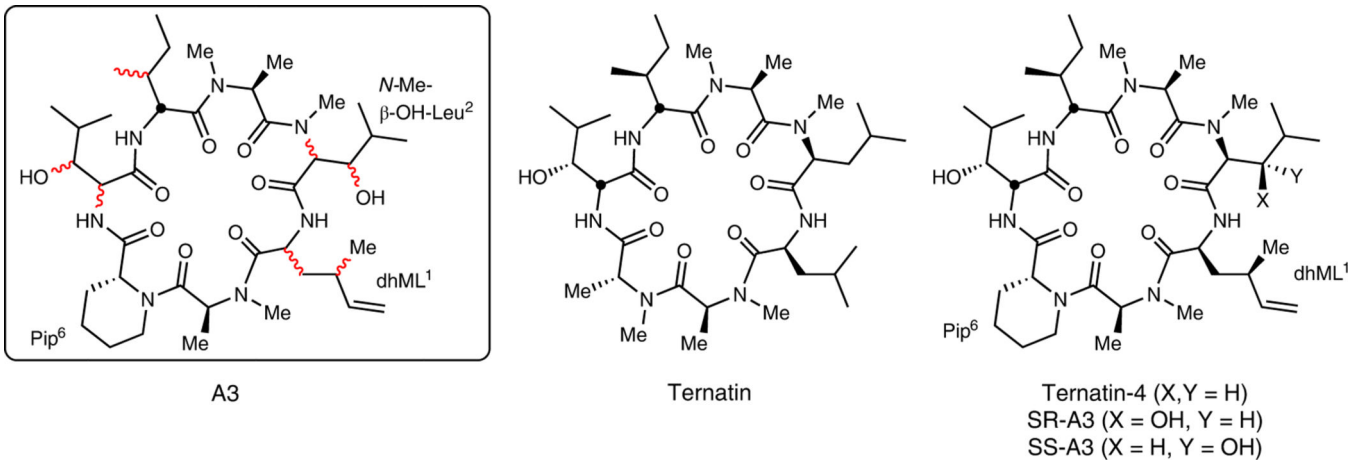

Figure 1. Partially determined structure of the natural product A3.

We hypothesized that A3 corresponds to one of two epimers – SR-A3 or SS-A3 – related to ternatin, a natural product, and ternatin-4, an A3-inspired synthetic compound.[14] Pip, pipecolic acid.

Author Manuscript Author Manuscript Author Manuscript Author Manuscript

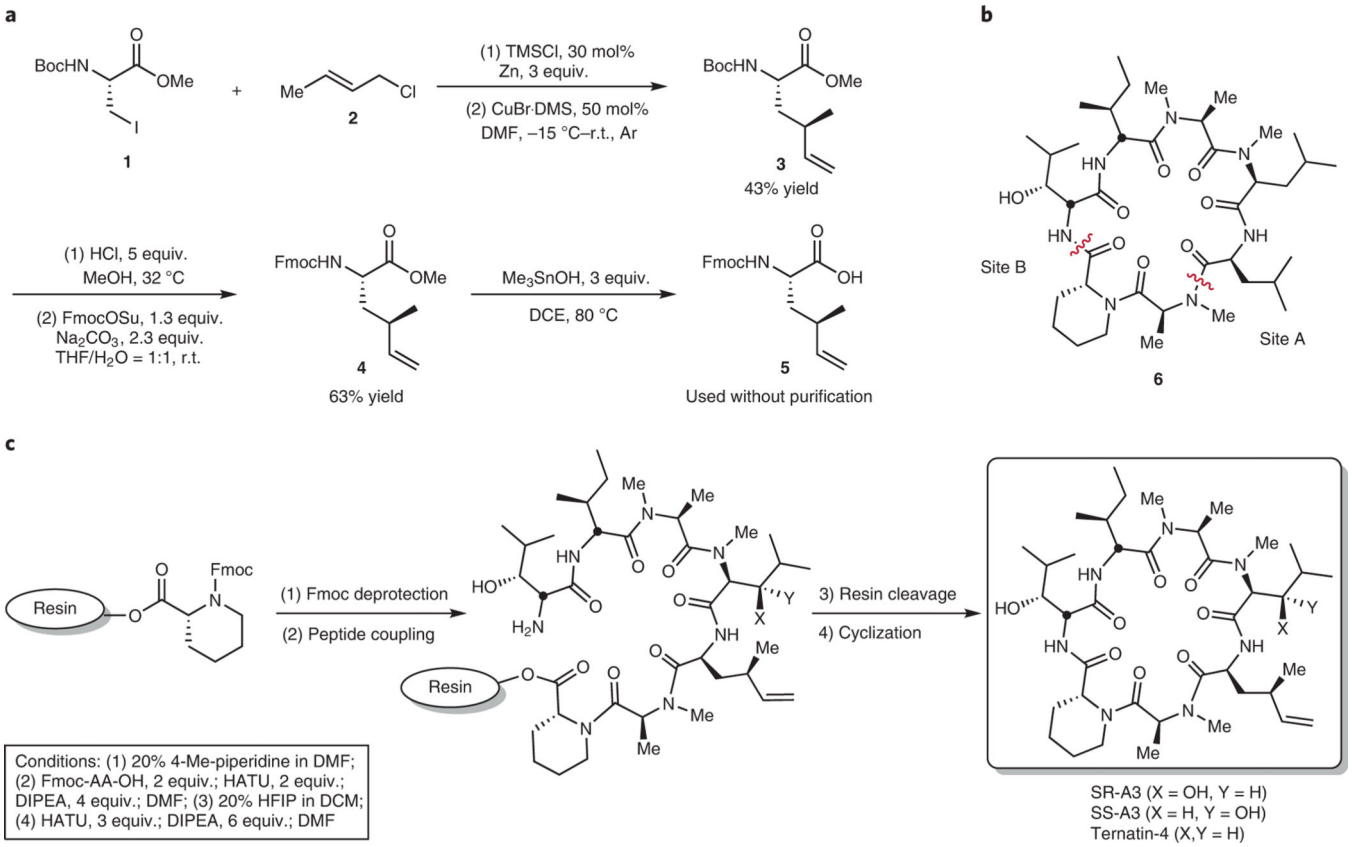

Figure 2. Expeditious synthesis of dhML, ternatin-4, and A3 epimers.

(**a**) Scheme for synthesis of Fmoc-dhML **5**. (**b**) Identification of alternative macrocyclization site B. (**c**) Scheme for solid-phase synthesis of linear heptapeptide precursors, followed by solution-phase cyclization to provide ternatin-4, SR-A3, and SS-A3 (see Supplementary Information for details). AA, amino acid; HATU, 1-[Bis(dimethylamino)methylene]-1H-1,2,3-triazolo[4,5-b] pyridinium 3-oxid hexafluorophosphate; DIPEA, N,N-Diisopropylethylamine; HFIP, 1,1,1,3,3,3-Hexafluoro-2-propanol; DCM, dichloromethane.

Author Manuscript Author Manuscript Author Manuscript Author Manuscript

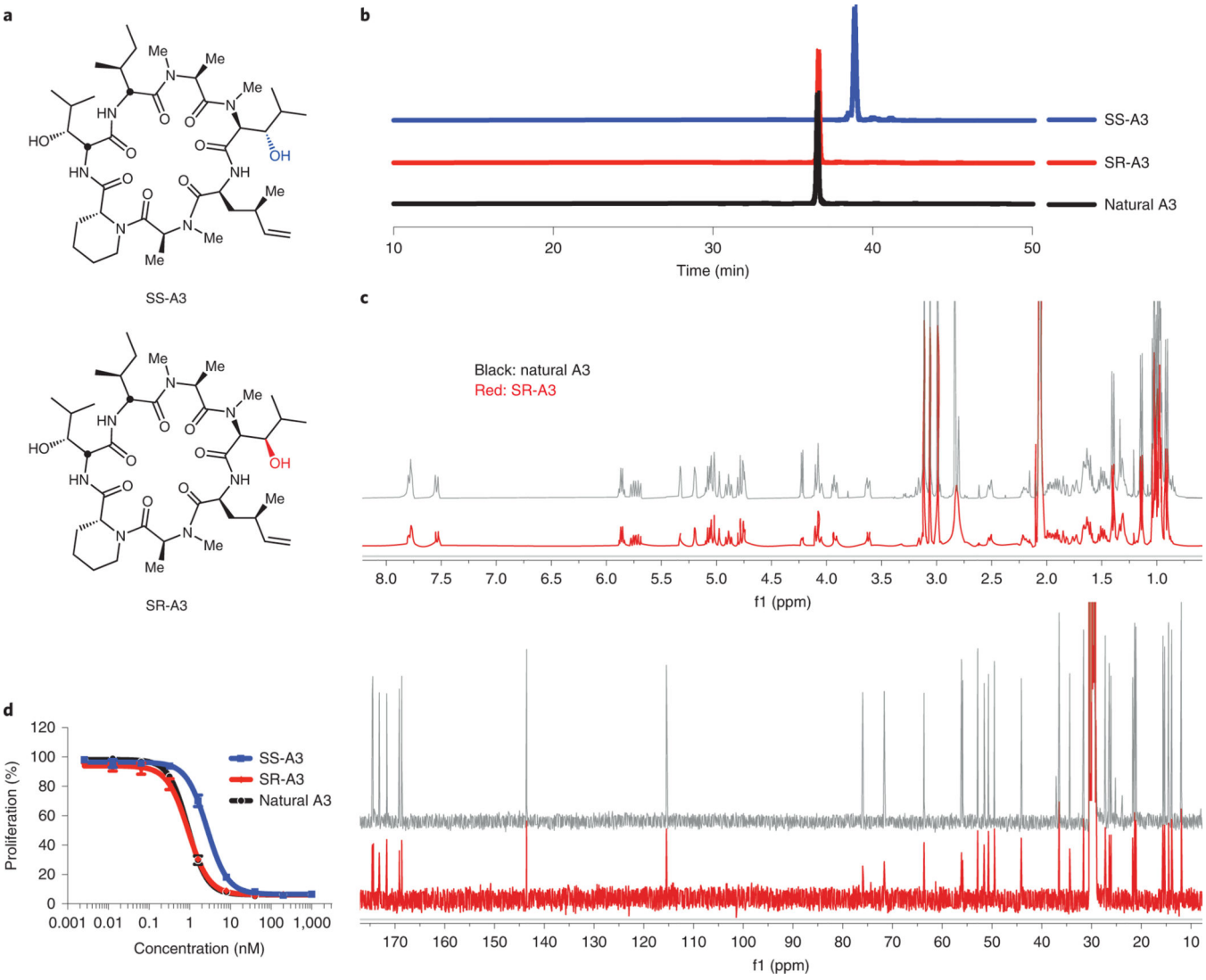

Figure 3. SR-A3 is indistinguishable from naturally derived A3.

(**a**) Chemical structures of SS-A3 and SR-A3. (**b**) HPLC elution profiles. (**c**) Overlay of ^{1}H and ^{13}C NMR spectra in acetone-d_6. (**d**) Concentration-dependent antiproliferative effects in HCT116 cells after 72 h. Cell proliferation (% DMSO control) was quantified using alamarBlue. Data points (% DMSO control) are mean values ± SD (n = 3).

Author Manuscript Author Manuscript Author Manuscript Author Manuscript

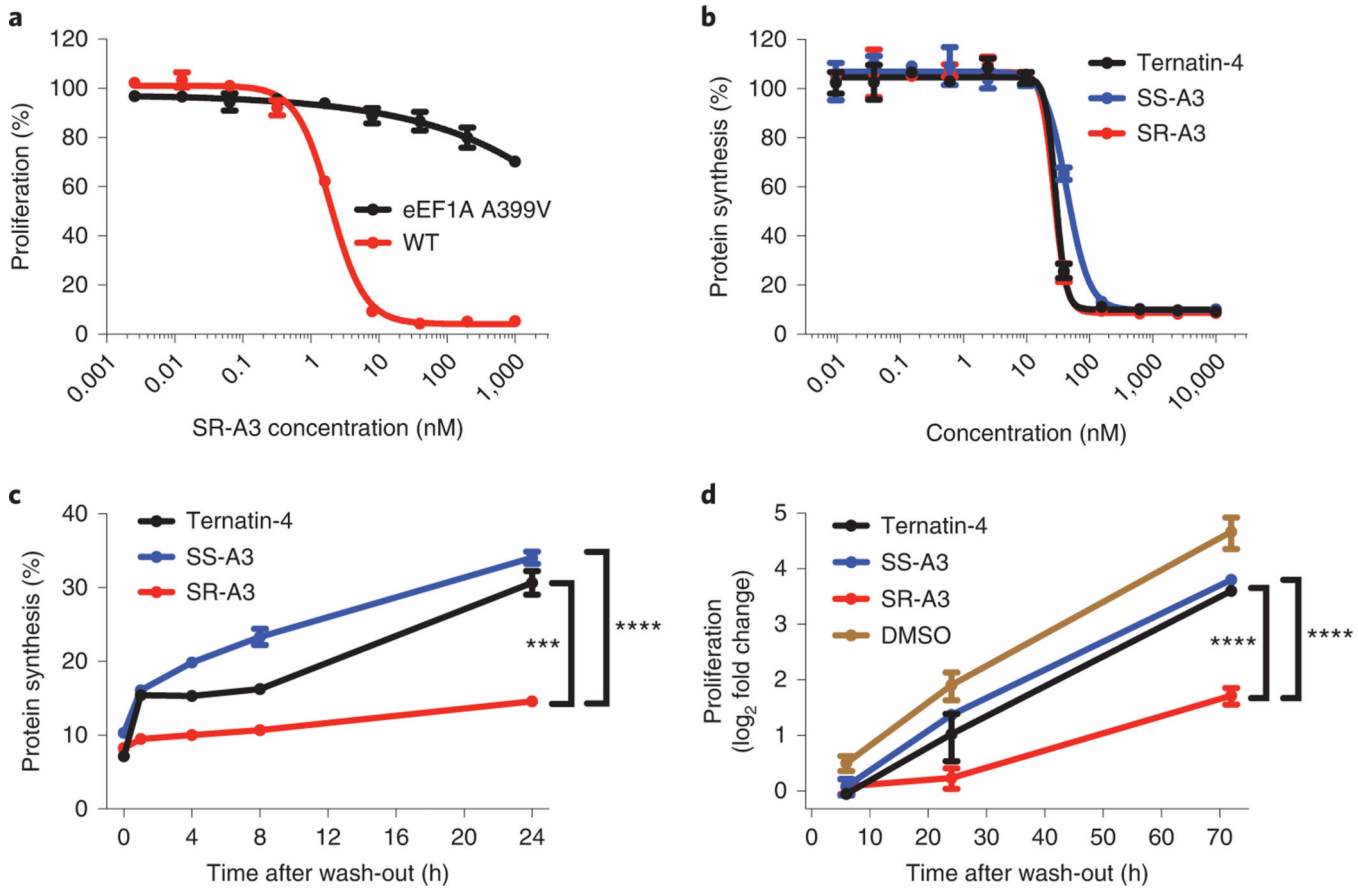

Figure 4. *N*-Me-β-OH-Leu stereospecifically endows SR-A3 with increased cellular residence time.

(**a**) Wild-type and eEF1A-mutant (A399V) HCT116 cells were treated with SR-A3 for 72 h. Cell proliferation (% DMSO control) was quantified using alamarBlue. Data points are mean values ± SD (n = 3). (**b**) HCT116 cells were treated with the indicated compounds for 24 h and protein synthesis was quantified after pulse labeling with *O*-propargyl puromycin for 1 h (see Methods). Data points (% DMSO control) are mean values ± SD (n = 3). (**c**) HCT116 cells were treated with the indicated compounds (100 nM) or DMSO for 4 h, followed by washout into compound-free media. At the indicated time points post-washout, cells were pulse-labeled with OPP (1 h), and OPP incorporation was quantified. Normalized data (% DMSO control) are mean values ± SD (n = 3). Statistical significance was determined by one-way ANOVA followed by Sidak's multiple comparisons test. ***, $P < 0.001$; ****, $P < 0.0001$. The P value for SR-A3 versus ternatin-4 is 0.0001. The P value for SR-A3 versus SS-A3 is < 0.0001. (**d**) HCT116 cells were treated with the indicated compounds (100 nM) or DMSO for 4 h, followed by washout into compound-free media. At the indicated time points post-washout, cell proliferation was quantified using the CellTiter-Glo assay. Normalized data (log2 fold change vs. DMSO control at t = 0 h post-washout) are mean values ± SD (n = 3). Statistical significance was determined by one-way ANOVA followed by Sidak's multiple comparisons test. ****, $P < 0.0001$. The P value for SR-A3 versus ternatin-4 is < 0.0001. The P value for SR-A3 versus SS-A3 is < 0.0001.

Author Manuscript Author Manuscript Author Manuscript Author Manuscript

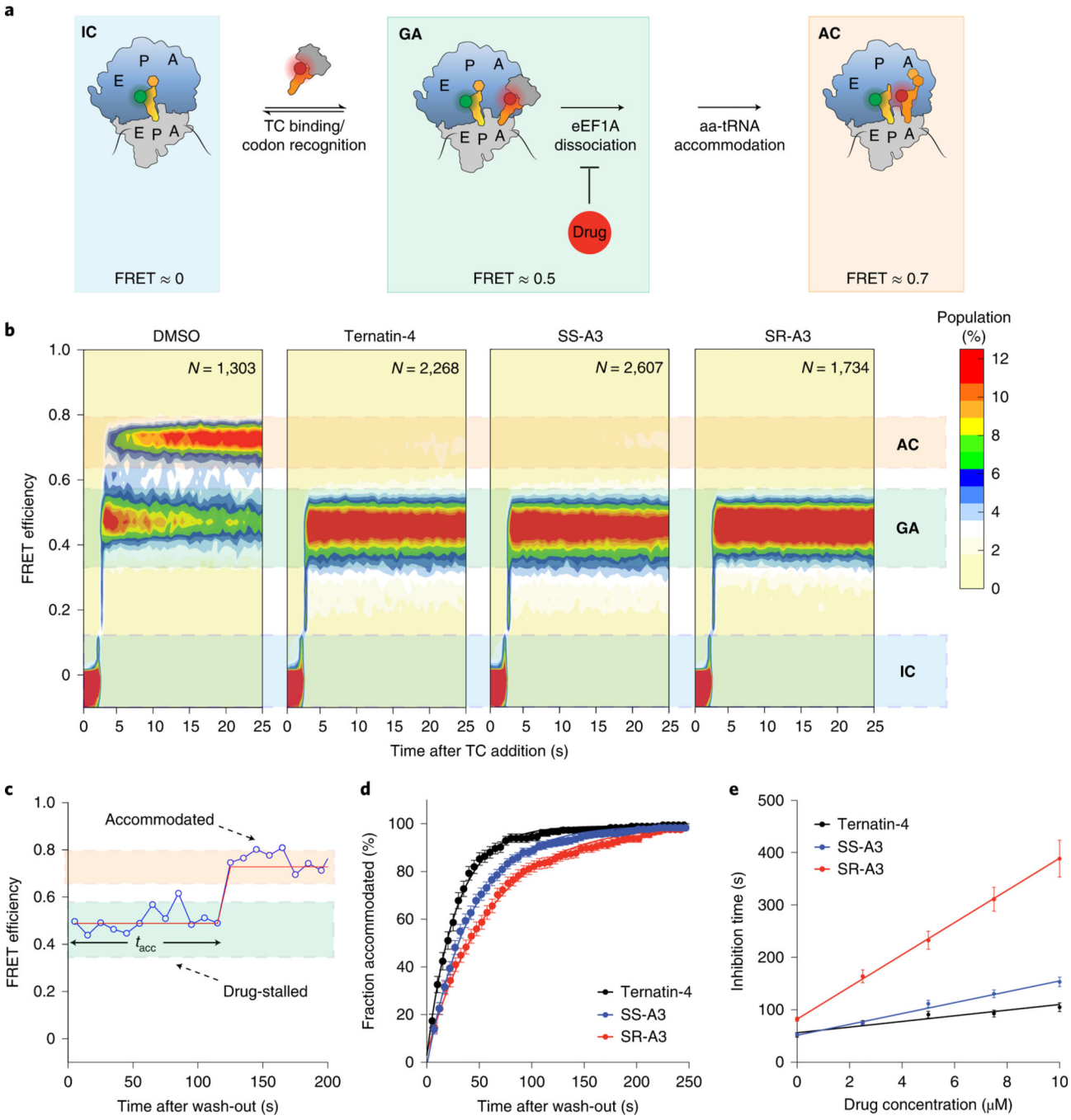

Figure 5. Single-molecule FRET imaging reveals increased residence time and rebinding kinetics of SR-A3.

(**a**) Schematic showing predominant long-lived reaction species (**IC, GA, and AC**) detected by the experimental setup. (**b**) Population FRET histograms of reactions initiated from **IC** by delivering the ternary complex (TC) and either DMSO or the indicated drug (10 μM) at the start of data acquisition. N = number of observed molecules. (**c**) Representative smFRET trace from a chase experiment initiated from drug-stalled elongation complexes (**GA**) by pre-incubation with SR-A3, followed by washout into drug-free buffer at the start of data

Author Manuscript Author Manuscript Author Manuscript Author Manuscript

acquisition. Blue circles represent the measured FRET efficiency for each movie frame; the solid red line represents a Hidden-Markov model idealization of the data. (**d**) Cumulative drug dissociation time distributions constructed from several thousand FRET traces as in (**c**) after washout into drug-free buffer. Data points represent bootstrap means (± SEM) from all FRET traces acquired in a single movie. The solid lines represent fits of single-exponential functions to the data (n = 3). (**e**) Plots of inhibition time (prior to accommodation) as a function of drug concentration in the washout buffer were used to determine drug residence times and rebinding constants. Inhibition times were derived from curves exemplified in (**d**), after washout into buffer containing the indicated drug concentrations. Each data point represents the mean of three independent experiments (± SEM, n = 3). Solid lines are linear fits to the data, adjusted R^2 = 0.90 (ternatin-4), 0.98 (SS-A3), and 0.99 (SR-A3). R^2, coefficient of determination.

Author Manuscript Author Manuscript Author Manuscript Author Manuscript

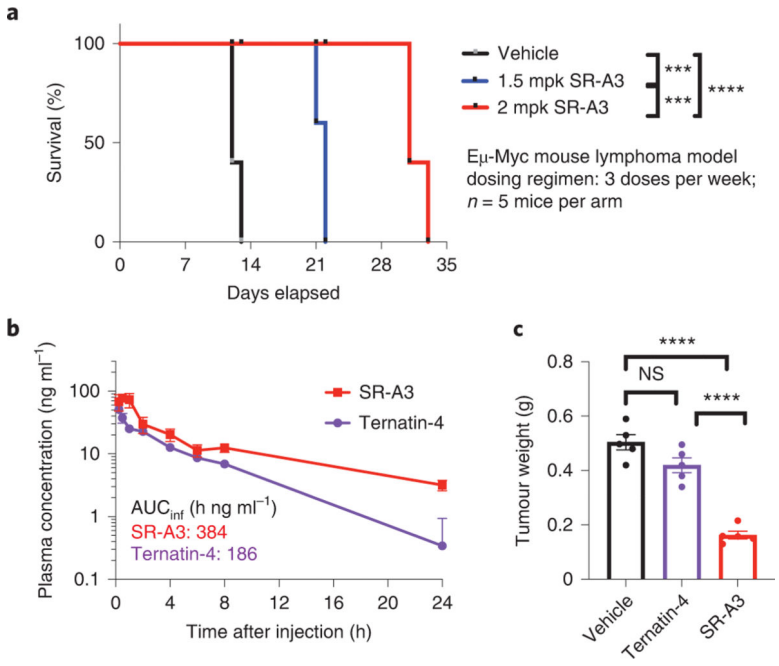

Figure 6. SR-A3 extends overall survival and reduces tumor burden in the Eμ-Myc mouse lymphoma model.

(**a**) Kaplan-Meier survival curves for mice dosed with vehicle or the indicated doses of SR-A3 (intraperitoneal injection, 3 times per week, n = 5 per dose group). Day 0 indicates the beginning of treatment. Statistical significance was determined by logrank test. ***, $P < 0.001$; ****, $P < 0.0001$. The P value for 2 mpk SR-A3 versus vehicle is < 0.0001. The P value for 2 mpk SR-A3 versus 1.5 mpk SR-A3 is 0.0001. The P value for 1.5 mpk SR-A3 versus vehicle is 0.0002. (**b**) Mouse plasma concentrations of SR-A3 or ternatin-4 after intraperitoneal injection at 2 mg/kg (mean ± SD, n = 3 mice per time point). (**c**) Tumor weights from Eμ-Myc mice after 2 weeks of treatment with vehicle, ternatin-4 (4.2 mg/kg), or SR-A3 (2 mg/kg) (n = 5 per group). Graph represents mean value ± SD. Statistical significance was determined by one-way ANOVA followed by Sidak's multiple comparisons test. ns, not significant; ****, $P < 0.0001$. The P value for SR-A3 versus vehicle is < 0.0001. The P value for SR-A3 versus ternatin-4 is <0.0001. The P value for ternatin-4 versus vehicle is 0.0708.